Lagrangian Motion, Coherent Structures, and Lines of Persistent Material Strain

R.M. Samelson

College of Earth, Ocean, and Atmospheric Sciences, Oregon State University, Corvallis, Oregon 97331-5503; email: rsamelson@coas.oregonstate.edu

Annu. Rev. Mar. Sci. 2013. 5:137–63

First published online as a Review in Advance on August 16, 2012

The *Annual Review of Marine Science* is online at marine.annualreviews.org

This article's doi: 10.1146/annurev-marine-120710-100819

Keywords

geophysical fluid dynamics, mesoscale dynamics, parcel motion, modeling

Abstract

Lagrangian motion in geophysical fluids may be strongly influenced by coherent structures that support distinct regimes in a given flow. The problems of identifying and demarcating Lagrangian regime boundaries associated with dynamical coherent structures in a given velocity field can be studied using approaches originally developed in the context of the abstract geometric theory of ordinary differential equations. An essential insight is that when coherent structures exist in a flow, Lagrangian regime boundaries may often be indicated as material curves on which the Lagrangian-mean principal-axis strain is large. This insight is the foundation of many numerical techniques for identifying such features in complex observed or numerically simulated ocean flows. The basic theoretical ideas are illustrated with a simple, kinematic traveling-wave model. The corresponding numerical algorithms for identifying candidate Lagrangian regime boundaries and lines of principal Lagrangian strain (also called Lagrangian coherent structures) are divided into parcel and bundle schemes; the latter include the finite-time and finite-size Lyapunov exponent/Lagrangian strain (FTLE/FTLS and FSLE/FSLS) metrics. Some aspects and results of oceanographic studies based on these approaches are reviewed, and the results are discussed in the context of oceanographic observations of dynamical coherent structures.

1. INTRODUCTION

Ever since Odysseus encountered the vortex Kharybdis in *The Odyssey* (circa 800 BCE), and no doubt long before, coherent structures such as nonlinear waves, meandering jets, and long-lived vortices or eddies have been familiar elements in descriptions of fluid flow in general and ocean circulation in particular. Although lacking a precise definition, these coherent structures are typically energetic vortical features with an organized spatial structure that remains recognizable for relatively long periods compared with other timescales in the flow, and as such are readily identified in a given flow (see, e.g., Hussain 1983, McWilliams 1984). Because of their constancy, such coherent features generally exert a sustained control over the motion of fluid parcels.

For the purposes of characterizing Lagrangian motion, the problem of locating the boundaries of coherent structures is of special importance. Indeed, one of the fascinating elements of fluid motion is that it may be so heterogeneous despite the near homogeneity of the fluid medium itself: Long-lived nonlinear jets and vortices that may transport fluid great distances, either by advection within a jet or by translation of a fluid-trapping vortex, may coexist side by side with relatively quiescent regions of flow in which the fluid parcels move, if at all, only in weak, nearly linear wavelike oscillations. Thus the future fate of a fluid parcel—whether it rocks gently back and forth in confined environs or makes haste toward distant parts of the field—may depend sensitively on its precise present position relative to these internal structures of the flow.

In a flow that is dominated by coherent structures, it is by passage through a coherent-structure boundary that the basic character of a fluid parcel's motion changes and the exchange of fluid between flow regimes occurs. Thus the demarcation of coherent structures through the definition of flow-regime boundaries becomes a natural goal of Lagrangian-motion analysis. The structures that most usefully describe the Lagrangian regime boundaries are, in general, Lagrangian objects themselves—that is, they are composed of material curves, sets of points that move with the fluid. The original work focusing on these material regime-boundary curves drew on the analogy between fluid flow and the abstract flows of the geometric theory of differential equations, in which bounding curves or surfaces can be defined that divide the phase space into distinct regions of dynamical behavior. The separatrices of a perfect rigid-rod pendulum are a simple example of the latter. These separatrices are the trajectories that asymptote to the unstable steady state in which the pendulum weight is directly above the axis of suspension, and separate the reversing oscillations about the stable, weight-down steady state from the monotonic rotations about the axis of suspension. The analogy and approach are particularly striking and effective when the fluid flow is two dimensional and divergence free, in which case material curves divide the plane of motion and the flow can be completely described by a time-dependent stream function that may be directly interpreted as the time-dependent Hamiltonian function of an abstract dynamical system.

A closely related problem is the determination of regions in which the persistent straining of material elements results in the efficient stirring of fluid property gradients to small scales, through the stretching and folding processes associated in the abstract setting with chaotic dynamics (e.g., Ottino 1989). It turns out that the material curves that compose Lagrangian regime boundaries are often lines of persistent Lagrangian strain, that is, sets of fluid elements that are subject to persistent straining as they move along their Lagrangian trajectories. Such lines of persistent material strain have become an object of study in themselves, independent of any direct connection to coherent structures, and are even sometimes denoted as Lagrangian coherent structures.

A number of methods have been proposed to identify Lagrangian regime boundaries in velocity fields obtained from ocean observations or numerical ocean circulation models. This review gives a brief introduction to some of the basic concepts and some of the methods used

to compute these structures, and provides a brief overview of some recent analyses that make use of this approach. These methods and the associated analyses have generally focused on two-dimensional, divergence-free conditions, which approximately hold for large classes of ocean flows. In many cases, the persistent material strain property is used to identify the corresponding material curves, and the connection to dynamical coherent structures may not be immediately apparent. In Section 2, a simple example is reviewed to give a concrete illustration of many of the basic concepts. Section 3 explores the connections between Lagrangian regime boundaries and lines of persistent material strain. Section 4 summarizes recent approaches to identifying these structures in observed or simulated ocean flows. Section 5 briefly reviews several oceanographic examples of the associated analyses. Section 6 provides a cursory overview of some recent results on the direct identification of dynamical coherent structures in the ocean, which do not rely on regime-boundary analyses but instead focus on the coherent-structure cores themselves. Section 7 concludes the review with a brief discussion and summary.

2. A KINEMATIC EXAMPLE: THE TRAVELING WAVE

Accessible examples of the basic Lagrangian structures are provided by the kinematic traveling-wave model (Samelson & Wiggins 2006). The traveling-wave flow is a two-dimensional, time-dependent velocity field described by a stream function $\psi(x, y, t)$, which consists of a traveling sinusoidal component ψ_0 plus a small perturbation $\varepsilon\psi_1$ that may take various forms:

$$\psi(x, y, t) = \psi_0(x, y, t) + \varepsilon\psi_1(x, y, t), \quad \psi_0(x, y, t) = A \sin k(x + ct) \sin ly. \tag{1}$$

In this equation, A is an amplitude, k and l are zonal (x) and meridional (y) wavenumbers, c is the wave-propagation speed (with $c > 0$ implying westward propagation), and $\varepsilon \ll 1$ is a small parameter. The flow is presumed to be confined to a zonal channel with rigid boundaries at $y = 0$ and $y = \pi/l$, where a no-normal-flow condition is satisfied by ψ_0 and imposed on ψ_1. This and closely related models have been explored by Flierl (1981), Knobloch & Weiss (1987), Pierrehumbert (1991), Samelson (1992), and others. In some cases, the relations between k, l, and c may be motivated by a dynamical linear wave theory, but the Lagrangian analysis may be carried out without regard to the dynamical origin or interpretation of the time-dependent stream function ψ, because ψ gives a complete description of the velocity field $\mathbf{u}(x, y, t)$ through the usual relation $\mathbf{u} = (u, v) = (-\partial\psi/\partial y, \partial\psi/\partial x)$.

Consider a reference frame (x', y') that is moving with the wave, so that

$$x' = x + ct, \quad y' = y. \tag{2}$$

With $\varepsilon = 0$, the fluid velocity $\mathbf{u}' = (u', v')$ in the comoving frame is given by

$$u' = \frac{\mathrm{d}x'}{\mathrm{d}t} = c + \frac{\mathrm{d}x}{\mathrm{d}t} = c - lA \sin kx' \cos ly', \quad v' = \frac{\mathrm{d}y'}{\mathrm{d}t} = \frac{\mathrm{d}y}{\mathrm{d}t} = kA \cos kx' \sin ly', \tag{3}$$

which is a steady flow described by a stream function $\psi_0'(x', y')$, where

$$\psi_0'(x', y') = -cy' + A \sin kx' \sin ly'. \tag{4}$$

The contours of the steady stream function ψ_0' are the streamlines of the flow (Equation 3) in the translating frame, and completely describe the Lagrangian motion when $\varepsilon = 0$. A characteristic geometry of these streamlines is illustrated by the case $A = k = l = 1$, $c = 0.5$ (**Figure 1**). In each zonal wavelength $\lambda = 2\pi/k = 2\pi$, there are two stagnation points on each of the $y = 0$ and $y = \pi/l = \pi$ boundaries, which are staggered in x' by $\lambda/2$. Each pair of stagnation points on a given boundary is connected by a contour that extends into the central region of the channel from

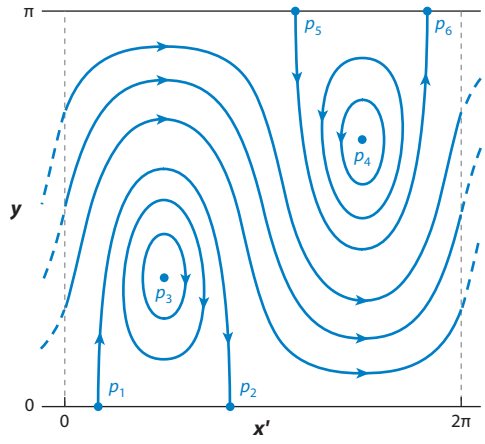

Figure 1

Steady streamlines in the comoving frame for the traveling-wave flow (Equations 1–3) for $A = 1$, $k = 1$, $c = 0.5$, and $\varepsilon = 0$. The channel is bounded by rigid walls at $y = 0$ and $y = \pi$. There are three flow regimes: two recirculation regions around the interior stagnation points p_3 and p_4 and a single central jet region between the recirculations. These regimes are separated by two special streamlines (*thick solid lines*) that join two pairs of stagnation points [(p_1, p_2) and (p_5, p_6)]. Only the segment $0 < x' < 2\pi$ is shown, corresponding to one wavelength of the traveling wave. Adapted from Samelson & Wiggins (2006) with kind permission from Springer Science+Business Media.

the upstream (western) point and then returns to the boundary at the downstream (eastern) point. An additional stagnation point is found inside each of the two regions enclosed by a segment of the boundary, a pair of stagnation points, and a connecting contour. The fluid parcels within the enclosed regions loop continuously around the interior stagnation points and are forever confined to the looping flow regimes. In contrast, the fluid parcels in the meandering jet between the two enclosed regions move continuously downstream, carried forever eastward in the jet flow regime.

This flow geometry, described by the steady stream function in the translating frame (**Figure 1**), can be compactly summarized by abstracting two sets of isolated material curves and points from the complete field of streamlines—one set for each of the two looping flow regions. Each set consists of a pair of stagnation points on one of the boundaries, the interior contours that connect them, and the boundary segments that complete the enclosure of the respective looping flow regime. These isolated elements apportion the fluid into looping and jet regimes, and so completely describe the qualitative character of the Lagrangian motion of any fluid parcel in the flow. The interior connecting contour, which forms most of the Lagrangian regime boundary, is known in the classical mathematical language as a separatrix, because it separates the two qualitatively different regimes of motion.

It is natural to ask whether a similar efficient description of the qualitative character of Lagrangian motion can be obtained for more general flows. A substantial number of the studies discussed here have been addressed at answering this question. The basic generalizations can be illustrated in the context of the traveling-wave flow (Equation 1). If additional, oscillatory time dependence is added to the steady moving-frame velocity field (Equation 3) by considering $\varepsilon > 0$ and a suitable form for ψ_1 in Equation 1, then the boundaries between the looping and jet flow regimes will be broken and will become porous to an exchange that scales with ϵ and the amplitude of ψ_1. In this case, generalized Lagrangian regime boundaries may often still be defined, and can then be used to quantify the exchange flux between the now time-dependent regimes

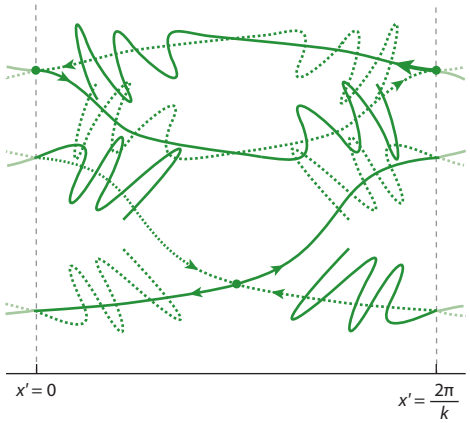

Figure 2

Schematic illustration of the breakup of the regime boundaries in a moving frame under the influence of time-dependent disturbances. As in **Figure 1**, the model is periodic in a direction parallel to the mean flow, so that the right and left boundaries of the figure may be identified. In this illustration, the traveling-wave flow is embedded in a resting ambient fluid rather than confined between rigid channel walls as in **Figure 1**, and each pair of boundary stagnation points in **Figure 1** is represented by a single stagnation-point analog at the edge of a recirculation regime. Adapted from Samelson & Wiggins (2006) with kind permission from Springer Science+Business Media.

(**Figure 2**). There are two parts of this generalization (e.g., Samelson & Wiggins 2006): First, suitable analogs of the boundary stagnation points must be found, and second, a set of bounding curves associated with these analog points must be defined that separate the flow into distinctive regimes of Lagrangian motion.

3. REGIME BOUNDARIES AND PRINCIPAL LAGRANGIAN STRAIN LINES

For a two-dimensional velocity field (u, v), the velocity gradient tensor $\mathbf{G}$ at point (x, y) may be written as

$$\mathbf{G} = \begin{pmatrix} \delta_1 & \gamma - \zeta \\ \gamma + \zeta & \delta_2 \end{pmatrix}, \tag{5}$$

where

$$\delta_1 = \frac{\partial u}{\partial x}, \delta_2 = \frac{\partial v}{\partial y}, \gamma = \frac{1}{2}\left(\frac{\partial u}{\partial y} + \frac{\partial v}{\partial x}\right), \text{ and } \zeta = \frac{1}{2}\left(\frac{\partial v}{\partial x} - \frac{\partial u}{\partial y}\right). \tag{6}$$

The eigenvalues σ_G and eigenvectors $\mathbf{x}^{\mathbf{G}}$ of $\mathbf{G}$ satisfy

$$\mathbf{G}\mathbf{x}^{\mathbf{G}} = \sigma_G \mathbf{x}^{\mathbf{G}} \tag{7}$$

and will be real if $s_{OW}^2 > 0$ and complex if $s_{OW}^2 < 0$, where the Okubo-Weiss parameter s_{OW}^2 is

$$s_{OW}^2 = \frac{1}{4}(\delta_1 - \delta_2)^2 + \gamma^2 - \zeta^2. \tag{8}$$

From a physical point of view, the case of real σ_G and $s_{OW}^2 > 0$ corresponds to a local motion field near the point (x, y) that is dominated by irrotational, straining deformation, whereas the case of complex σ_G and $s_{OW}^2 < 0$ corresponds to a local motion field that is dominated by vorticity and rotation.

In the steady traveling-wave flow (Equation 3), the Lagrangian regime boundaries that separate the looping and jet regimes turn out to have a second identity as material lines of large Lagrangian-mean strain. The interior stagnation points are surrounded by closed, elliptical streamlines, with nearby fluid parcels looping endlessly about the stagnation points and essentially no local mean straining motion (**Figures 1** and **2**). Consequently, the Lagrangian-mean strain for a looping trajectory near either interior stagnation point will be essentially zero. In addition, the Lagrangian-mean strain for trajectories following the central jet will likewise be relatively small, because the (Eulerian) strain vanishes at the center of the jet. This is not the case, however, for the separatrix trajectories or their time-dependent generalizations.

Because the sets of parcels that form each separatrix are those with trajectories that asymptote toward the boundary stagnation points, the Lagrangian-mean average strain properties on these parcels over long time intervals are dominated by the strain properties of the respective stagnation points. For the forward semi-infinite mean, over times t with $t_0 < t < \infty$ for any fixed t_0, the Lagrangian-mean principal strain along such a trajectory will be dominated by that of the downstream stagnation point; for the backward semi-infinite mean, over times t with $-\infty < t < t_0$ for any fixed t_0, the Lagrangian-mean principal strain along such a trajectory will be dominated by that of the upstream stagnation point. Thus, in a Lagrangian sense, the large material strain rates at the boundary stagnation points will effectively extend into the interior as large Lagrangian-mean principal strain rates for the parcels on each separatrix.

The material strain properties at the boundary stagnation points are determined by the surrounding linear deformation fields, which have principal axes aligned along the directions in which nearby fluid parcels approach the stagnation points asymptotically in infinite forward or backward time (**Figure 1**). The fluid parcel at a boundary stagnation point, by virtue of its stationary position at the center of the linear deformation field, is subject to a persistent straining motion from the corresponding deformation field. Nearby fluid parcels that approach the downstream boundary stagnation point on opposite sides of the separatrix will depart exponentially fast from each other and from the stagnation point in forward time, or will approach each other and the point exponentially in backward time. A similar picture holds at the upstream stagnation point, but with time reversed. It is this exponential rate of separation or approach that is quantified by the principal rates of strain at the stagnation point and that dominates the forward-time or backward-time Lagrangian-mean normal strain for parcels on the separatrix. Thus, because of the persistent large strain that occurs as the separatrix parcels approach or leave the boundary stagnation points, the separatrices are lines of large Lagrangian-mean strain.

For the weakly unsteady traveling-wave flow—that is, Equation 1 with $0 < \varepsilon \ll 1$ and a suitable oscillatory form for ψ_1—a similar relation holds: The generalized Lagrangian regime boundaries can again be identified as material lines of large Lagrangian-mean strain. In this case, the separatrix is replaced by two sets of material lines, composed separately of the parcels with trajectories that asymptote to the analogs of the upstream and downstream boundary stagnation points (**Figure 2**) (see also, e.g., Samelson & Wiggins 2006). The parcels that in forward time approach the analog of the downstream point will have a large, normally divergent, principal Lagrangian-mean strain, whereas those that in backward time approach the analog of the upstream point will have a large, normally convergent, principal Lagrangian-mean strain. The former is normally divergent and the latter normally convergent in the sense that they indicate, respectively, Lagrangian-mean divergence from and convergence toward the corresponding material lines, in forward time.

This heuristic insight—that when coherent structures exist in a flow, the Lagrangian regime boundaries tend to be indicated as material lines of large Lagrangian-mean strain—has formed the

foundation of many attempts to identify the Lagrangian regime boundaries of coherent structures in complex flows (see Section 4). It should be borne in mind, however, that although coherent-structure regime boundaries may indeed often have a large Lagrangian-mean strain, it is not necessarily the case that, conversely, all material lines of large Lagrangian-mean strain are themselves Lagrangian regime boundaries. In fully developed turbulence, for example, where eddy lifetimes are comparable to Lagrangian decorrelation times, material lines of large Lagrangian-mean strain may have an exceedingly complex geometry with no clear connection to any identifiable localized Lagrangian-motion regimes (e.g., Mathur et al. 2007).

Because of the importance of repeated or sustained material deformation to the analysis of stirring or mixing in fluid flows, material lines of large Lagrangian-mean strain are an object of interest themselves, regardless of their possible role as Lagrangian regime boundaries in flows with coherent structures. In reflection of this intrinsic importance, these lines have sometimes themselves been called Lagrangian coherent structures (LCSs) (Haller & Yuan 2000). In the present geophysical fluid-dynamical context, however, in which the term coherent structure has an established meaning as a localized, quasi-stable, vortex-dynamical feature, the LCS terminology can lead to confusion. The LCS terminology is therefore avoided here in favor of the more explicitly descriptive term principal Lagrangian strain (PLS) line.

4. SCHEMES AND ALGORITHMS

4.1. The Contoured-Field Approach

In simple examples such as traveling-wave flow (Equation 1), in which the unperturbed velocity field is analytically specified and time independent in a suitable reference frame, the fixed points and separatrices can be easily identified. For a general velocity field, obtained from ocean observations or numerical ocean-model simulations, the identification problem is challenging. A number of different identification schemes and algorithms have been proposed and explored. Initially, many of these focused on finding approximate stagnation points through iterative methods initialized with the locations of instantaneous points of zero velocity (Ide et al. 2002). However, such instantaneous stagnation-point schemes have typically been strongly frame dependent and difficult to automate. For example, any trajectory will appear to be a stagnation point in a moving frame that follows the trajectory, and some relative measure of parcel motion is needed to remove this basic ambiguity. A more successful and now widely used approach involves computing various Lagrangian-mean quantities on a large number of trajectories, contouring the resulting field, and finding the contours with extremal values. Because the contoured-field approaches are explicitly relative, in that the identified features are defined by extremal rather than absolute values, they implicitly have an approximate Galilean (or more general) frame invariance, and so automatically satisfy, at least approximately, this fundamentally important criterion for any candidate scheme.

The Lagrangian-mean, trajectory-based, contoured-field approaches may be divided into two categories: parcel schemes and bundle schemes. The former are based on Lagrangian means of primary flow quantities, such as velocity, and so can be evaluated from information along an individual parcel trajectory. [Rypina et al. (2010) refer to parcel schemes as "individual trajectory methods," although, of course, the quantities must be computed for a field of trajectories in order to yield meaningful results.] The latter involve Lagrangian means of spatially differentiated quantities, such as velocity gradients, and so effectively require information on a surrounding (infinitesimal, open) set of neighboring trajectories. The word bundle may here be interpreted to connote either the required groups of neighboring trajectories or perhaps the more abstract

mathematical notion of a tensor bundle (e.g., Bishop & Goldberg 1980; strictly speaking, of course, the parcel velocity is already an element of a tangent bundle). From a mathematical point of view, the problem of identifying extremal contours might be anticipated to have a natural formulation as a variational problem; this approach has recently been taken by Haller (2011), who derived results for a bundle scheme. A gradient-based iterative scheme to locate the extremal contours in complicated Lagrangian-mean fields has been developed by Mathur et al. (2007).

The results of a Lagrangian-mean, contoured-field scheme may be extended by computing stagnation-point and separatrix analogs, generally by iterative methods (Haller 2000, 2001, 2002; Ide et al. 2002; Mancho et al. 2003, 2004, 2006), with an intersection point of extremal contours of the Lagrangian-mean fields used as an initial guess. The appropriate analogs of the stagnation points have been called "distinguished hyperbolic trajectories" (Ide et al. 2002), but this abstract terminology conveys little physical information. Their essential characteristic is a persistent local strain field, similar to that of the boundary stagnation points in the traveling-wave flow, which can support the asymptotic approach of fluid parcels in forward or backward time; therefore, the more explicitly descriptive term PLS point is used here instead. The separatrix analogs are composed at any given time of the fluid parcels that asymptote toward the PLS point in forward or backward time. In the abstract terminology, the separatrix analogs are called stable or unstable manifolds of the distinguished hyperbolic trajectory (PLS point), or, because they are composed of material points, they may be called simply material manifolds (Samelson & Wiggins 2006). Here, they are instead identified as either PLS lines or Lagrangian regime-boundary curves.

4.2. Parcel Schemes

As defined here, parcel schemes are those based on Lagrangian means of primary flow quantities along an individual parcel trajectory. Examples of such schemes are the mean Lagrangian velocity metric of Malhotra et al. (1998) and the recently proposed arc-length metric of Madrid & Mancho (2009).

The former measure is based on the mean Lagrangian velocity of a fluid parcel over a specified time interval, which is equal to the ratio of the distance between the final and initial positions of the parcel to the difference between the final and initial times (Malhotra et al. 1998). In a two-dimensional flow, this mean Lagrangian velocity is a vector, and the contoured quantity may be the magnitude of the vector or—especially if the flow is anisotropic, as is the case for the traveling-wave model—the value of one of the components of the vector (**Figure 3**). This metric is especially useful for identifying contiguous regions of flow with a characteristic shared Lagrangian behavior. Thus, it distinguishes relatively clearly between the jet and recirculation regimes in a traveling-wave flow (**Figure 3**). However, it is not especially well suited to the problem of identifying the boundaries between regimes, which is the primary goal.

The latter measure is constructed from the arc length of a finite-time parcel trajectory, defined at time t as the time mean over an interval $[t - \tau/2, t + \tau/2]$ of the Lagrangian integral of the magnitude of the parcel's velocity (Madrid & Mancho 2009). This metric (**Figure 4**) appears to provide a more sensitive indicator of the regime boundaries than the mean Lagrangian velocity itself. The essential reason for this difference is that the set of parcels forming the boundaries will have trajectories that asymptote toward some generalized analog of the boundary stagnation points in the traveling-wave flow, at which their motion often tends to decrease relative to other parts of the flow, whereas parcels that are looping repeatedly in recirculation regimes will continue to accumulate trajectory arc length even as their mean Lagrangian velocity relative to the translating frame decreases toward zero. Thus, unlike the mean Lagrangian velocity, the arc-length metric is able to distinguish between the recirculation regime and its boundary. Although this heuristic

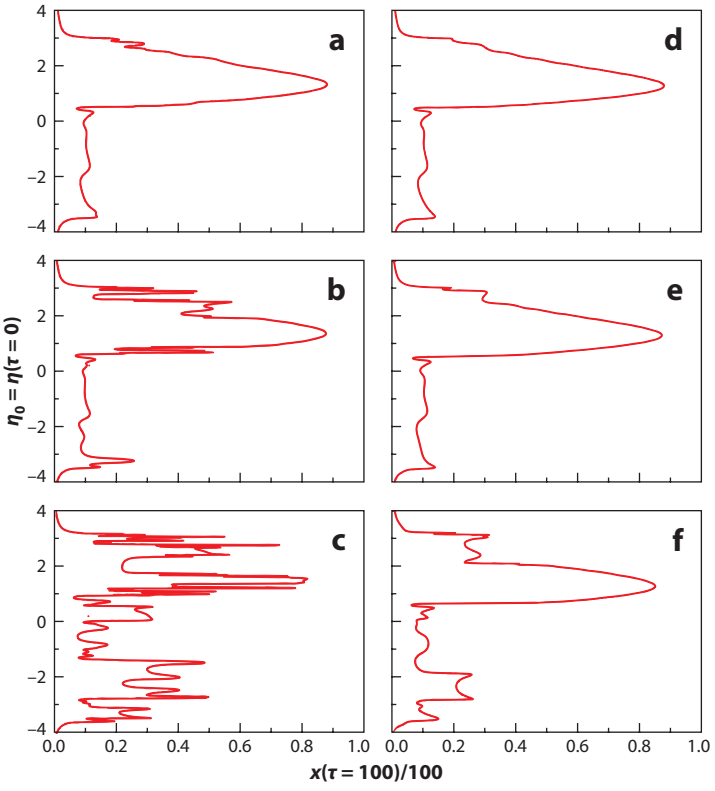

Figure 3

Cross section of a parcel-scheme metric similar to that of Malhotra et al. (1998) for a variant of the traveling-wave flow, showing long-term mean zonal (along-channel) Lagrangian velocity in the stationary frame for parcels initially on a section $x(\tau = 0) = 0$ near the wave-phase equivalent of $x' = \pi/2$ in **Figure 1**. For wave and perturbation parameters as in panels *a*, *b*, *d*, *e*, and *f*, the recirculation regime is characterized by a mean velocity near $c = 0.1$, whereas the jet regime is characterized by larger mean velocities. For parameters as in panel *c*, the coherent structures are barely evident. Adapted from Samelson (1992) with permission; original figure copyright © 1992 by the American Meteorological Society.

argument is suggestive, and practical results with this method have so far given encouraging results, a rigorous justification of its validity is not currently available.

4.3. Bundle Schemes

As defined here, bundle schemes are those based on Lagrangian means of spatially differentiated quantities along a parcel trajectory. The spatial differentiation may be approximated by discrete differences from two or more neighboring trajectories. Two bundle schemes that have received substantial attention are those based on finite-time Lyapunov exponents (FTLEs) (Ottino 1989, Pierrehumbert & Yang 1993, Haller 2001, Shadden et al. 2005) and finite-size Lyapunov exponents (FSLEs) (Aurell et al. 1997, d'Ovidio et al. 2004). The stagnation-point and bounding-trajectory analogs are then identified as ridges in the FTLE or FSLE fields. Most schemes have included explicitly Lagrangian parcel-tracking elements, but an Eulerian alternative has recently been proposed (Leung 2011) that uses the advection of Lagrangian labels (Kuebel Cervantes et al. 2003, 2004) to develop a numerical representation of the Lagrangian flow map. A variety of studies using

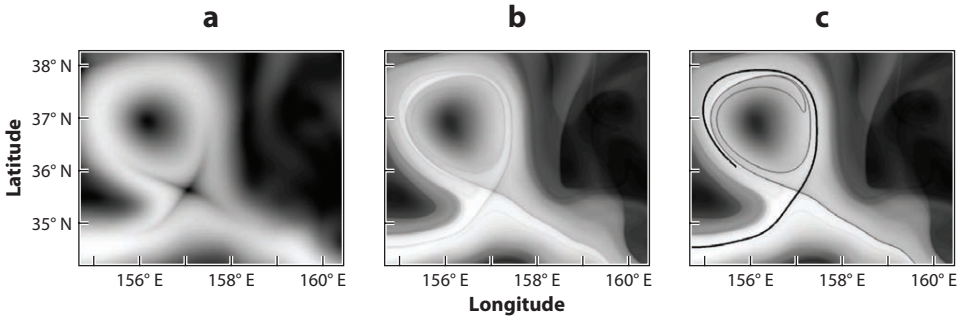

Figure 4

Arc-length metric (*shading*) computed following Madrid & Mancho (2009) from an observational ocean surface-velocity data set for intervals of (*a*) 4 and (*b*,*c*) 30 days. Panel *c* additionally plots segments of Lagrangian regime boundaries representing the stable (*black*) and unstable (*gray*) manifolds of the associated stagnation-point analogs. In panel *b*, note that the contoured values are similar inside and outside the enclosed recirculation regime (indicated by the light shading fading to dark farther inside and outside) and distinctively different along the regime boundaries (indicated by the dark shading along narrow, isolated curves embedded in light shading). Adapted from Mendoza & Mancho (2010) with permission; original figure copyright © 2010 by the American Physical Society.

variants of these schemes have given encouraging results, and in some cases further steps toward rigorous justification of these methods have been taken (Shadden et al. 2005, Haller 2011, Haller & Sapsis 2011).

The Lyapunov exponent terminology has been borrowed from dynamical systems theory, where this exponent describes the asymptotic instability of phase-space trajectories, with a positive exponent for a bounded system generally implying chaotic behavior (e.g., Guckenheimer & Holmes 1983). As a descriptor for the Lagrangian motion, however, it is disappointingly obscure. The FTLE quantity itself is in essence a Lagrangian-mean principal-axis strain rate along the given trajectory, estimated by finite differences. A more fluid-dynamical terminology for the FTLE might be finite-time Lagrangian strain (FTLS). The FSLE is effectively also a Lagrangian-mean principal-axis strain rate, computed instead from the time required to reach the specified separation. A more fluid-dynamical terminology for the FSLE might be finite-size Lagrangian strain (FSLS).

In the FTLE/FTLS approach, a fixed, finite time interval τ is chosen, and the FTLE/FTLS at time t is computed as a mean exponential growth rate of separations between two trajectories over the time $[t, t+\tau]$ by dividing the logarithm of the ratio of final to initial separations by τ (**Figure 5**). More generally, in two or more spatial dimensions, the computation can be done for a field of trajectories initialized on a regular grid, and a discrete-difference estimate of the Cauchy-Green deformation tensor can be computed along each trajectory and then diagonalized to obtain the corresponding eigenvalues, from which a maximum FTLE/FTLS can be computed by dividing the square root of the leading eigenvalue by τ (e.g., Shadden et al. 2005). In principle, the FTLE/FTLS asymptotes toward a Lyapunov exponent (e.g., Oseledec 1968) as $\tau \to \infty$, which provides the theoretical rationale for the name. A backward FTLE/FTLS may also be computed, over the time $[t+\tau, t]$ with $\tau < 0$.

In the FSLE/FSLS approach, the FTLE/FTLS scheme is, loosely speaking, inverted. Instead of the fixed time interval τ, a suitable ratio of final to initial separations between two trajectories is chosen a priori, and the time τ_S taken for the separation ratio to reach this specified value is recorded. The FSLE/FSLS is then defined as the mean exponential separation rate obtained by dividing the

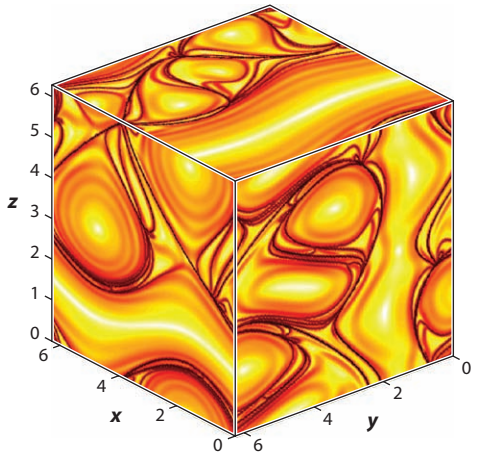

Figure 5

A finite-time Lyapunov exponent/Lagrangian strain (FTLE/FTLS) field for an analytic example consisting of a triply periodic, steady, three-dimensional velocity field. Darker colors indicate larger values. Local maxima indicate normally divergent principal Lagrangian strain (PLS) lines. Adapted from Haller (2000) with permission from Elsevier.

logarithm of the specified separation ratio by τ_S (**Figure 6**). In two or more spatial dimensions, τ_S for a given trajectory can be minimized over initial separation directions to obtain the corresponding maximum FSLE/FSLS. The FSLE/FSLS approach has the practical appeal of allowing explicit specification of the horizontal scales over which the separation rates are to be computed.

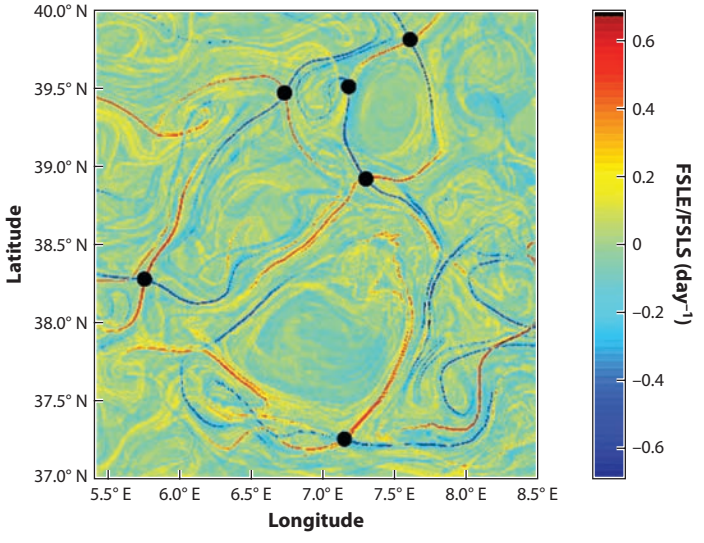

Figure 6

Finite-size Lyapunov exponent/Lagrangian strain (FSLE/FSLS) fields calculated from forward (*positive values*) and backward (*negative values*) integrations in time, for a time-dependent surface-velocity field from a numerical ocean model. Local maxima and minima indicate principal Lagrangian strain (PLS) lines. Black dots indicate possible positions of stagnation-point analogs at the PLS-point intersections of the PLS lines. Adapted from d'Ovidio et al. (2004) with permission.

5. OCEANOGRAPHIC EXAMPLES

5.1. Western Boundary Currents

Perhaps the most well-developed oceanographic exploration of the Lagrangian regime-boundary ideas is that associated with the North Atlantic's midlatitude western boundary current—i.e., the Gulf Stream and its offshore extension (Stommel 1965). The original work of Bower & Rossby (1989), Bower (1991), and Samelson (1992), which identified the characteristic traveling-wave flow structure of the meandering current and its implications for cross-jet fluid exchange, stimulated subsequent observational analyses with an increasing theoretical motivation, as well as numerical studies with increasingly realistic ocean models. Much of this work has previously been reviewed by Samelson (1996) and Wiggins (2005).

These studies have largely confirmed the essential perspectives and insights of the highly idealized traveling-wave representation of Lagrangian motion in a meandering jet. Technical elements of the approach have proven to be sound in a broader context, as evidenced, for example, by the utility of the comoving reference frame as a context for the analysis of observed trajectories of freely drifting subsurface floats deployed in the Gulf Stream (Lozier et al. 1997) and the demonstrated validity of the kinematic model as a qualitative representation of Lagrangian motion in dynamically based numerical models of meandering jets (Rogerson et al. 1999). Analysis of subsurface float motion in comoving reference frames defined independently through estimates of meander propagation speeds reveals trajectories whose qualitative exchange behavior is similar to that inferred from a variant of the traveling-wave flow (**Figure 7**) (Lozier et al. 1997). Numerical simulations using a barotropic vorticity equation as an idealized representation of Gulf Stream dynamics confirmed that the basic pathways of Lagrangian motion and fluid exchange arising in the traveling-wave flow also occur when the velocity field is determined from a consistent dynamical model based on a material conservation principle for the mesoscale vorticity (**Figure 8**) (Rogerson et al. 1999).

These studies of Lagrangian motion in the Gulf Stream have also produced several specific physical insights. For example, the qualitative and to some extent quantitative characteristics of exchange mechanisms and locations relative to meanders, and the intensification of cross-jet exchange with depth, are now seen as most naturally understood in the context of the traveling-wave model of Lagrangian motion and the dependence of this model's Lagrangian regime boundaries on such basic physical parameters as the ratio of the traveling wave's phase speed to the maximum flow speed in the jet. This emphasis on the Lagrangian boundaries between the recirculation and jet regimes as descriptors of the material motion in the Gulf Stream has proven to be a conceptual focus with lasting value.

5.2. Coastal Flow Regimes

A coastal flow regime that has received much attention from the Lagrangian perspective is the surface current field in and around Monterey Bay, California, on the US west coast. Extending previous work by Coulliette et al. (2007), Shadden et al. (2009) have used remote-sensing estimates of the surface current field from a land-based high-frequency (HF) radar system (Paduan & Rosenfeld 1996) during periods in July through September 2003 to compute Lagrangian regime boundaries (PLS lines) through an FTLE/FTLS approach, with comparisons to in situ surface drifter measurements. The horizontal scale of the domain was of order 20 km, the typical surface current speeds were of order 25–50 cm s^{-1}, and the integration time for the FTLE/FTLS approach was $\tau = 3$–4 days.

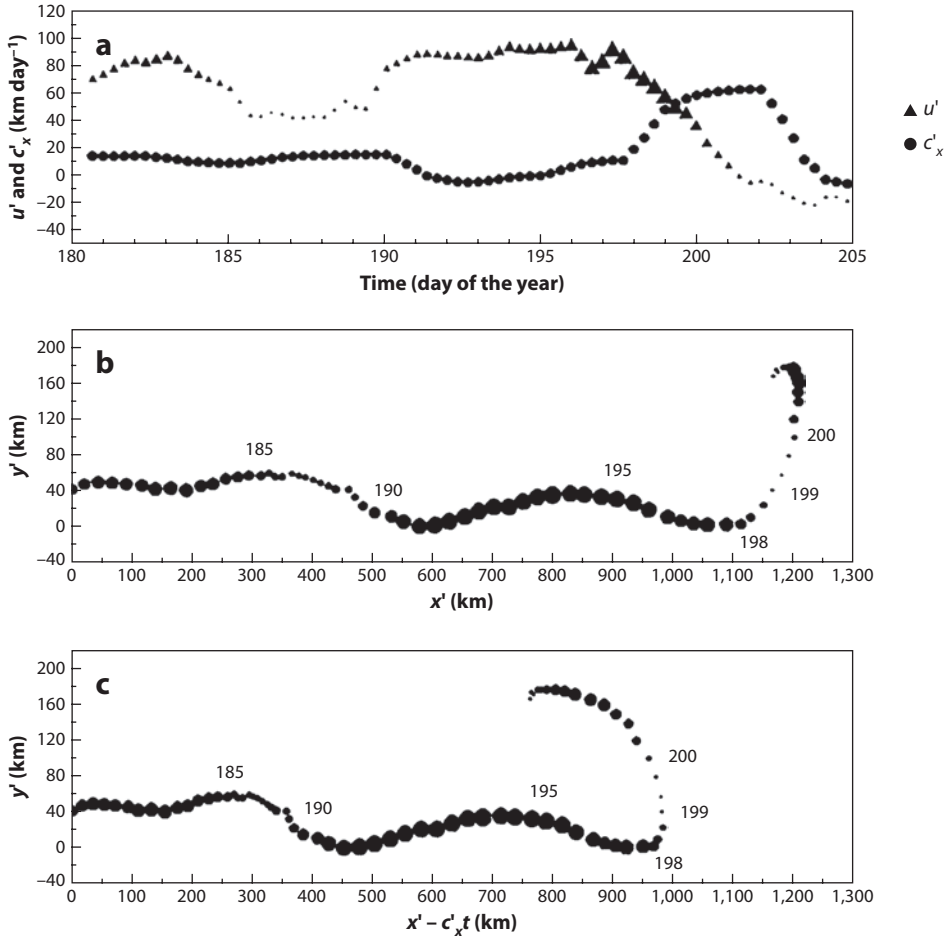

Figure 7

Subsurface motion data from RAFOS float 037. (*a*) Time series of float quasi-zonal speed u' (*triangles*) and estimated meander quasi-zonal phase speed c'_x (*circles*) for the portion of the float's life with phase speed coverage. For u', the size of the symbol is proportional to the pressure along the float's path. Small values denote small pressures (onshore side of the stream) and large values denote large values (offshore side of the stream). (*b*) Stationary-frame trajectory with symbol size proportional to $|u' - c'_x|$. (*c*) Moving-frame trajectory with symbol size proportional to $|u' - c'_x|$. The symbol spacing in all panels is 8 h. Adapted from Lozier et al. (1997) with permission; original figure copyright © 1997 by the American Meteorological Society.

The regime boundaries of interest tended to separate a recirculation flow within the bay from an offshore flow southward past its open mouth (**Figures 9** and **10**). The drifter trajectories were broadly consistent with the flow structure inferred from the PLS-line analysis, although significant quantitative differences were also found both between the drifter and inferred PLS-line positions and between the observed and predicted drifter positions, where the prediction was based on a single trajectory integration using the HF radar velocity field. Some of these discrepancies may have resulted from the relatively large depth to which the drogue element on the drifters extended, in comparison with the approximately 1-m depth of the HF radar current estimates. Shadden

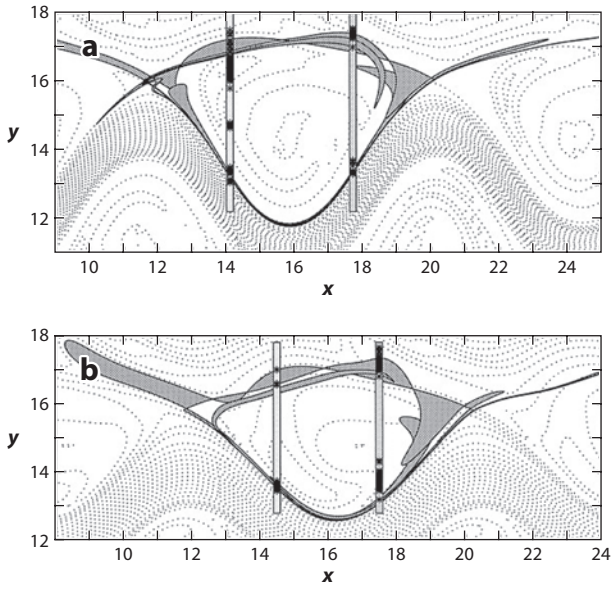

Figure 8

Composite illustrations of the potential vorticity field (*dotted-line contours*), fluid-exchange regions defined by Lagrangian regime boundaries (*shaded areas*), and two meridional transects through the recirculation region where Lagrangian particles are initially positioned 0.05 units apart for (*a*) case I at time $t = 98$ and (*b*) case III at time $t = 102$, where cases I and III denote two model simulations with differing parameter values. Panels *a* and *b* track a total of 242 and 202 particles, respectively, for 200 time units. The initial positions of particles that exhibit rapid potential vorticity transitions—$\Delta q > 0.01$ and $\Delta q > 0.015$ for panels *a* and *b*, respectively, over any 10-unit time interval, indicating enhanced stirring and mixing of potential vorticity—are marked within the vertical bars. Adapted from Rogerson et al. (1999) with permission; original figure copyright © 1999 by the American Meteorological Society.

et al. (2009) argued that the PLS-line estimates were relatively robust because the Lagrangian integrals used for the FTLE/FTLS computation act to smooth, or filter, the noise in the observed HF radar velocity fields. They further suggested that the PLS-line pattern along the mouth of the bay may be consistently related to sustained, wind-driven coastal upwelling conditions (**Figures 9** and **10**). This is an example of a potentially useful and testable description of the characteristic regional Lagrangian response to wind forcing that is posed with particular efficiency in the present framework.

5.3. Eastern Boundary Currents

The California Current System (CCS) is an eastern boundary current regime with an active mesoscale eddy field, located roughly 100–300 km offshore of the US west coast, including the region to the west of the coastal embayment regime considered by Shadden et al. (2009). Harrison & Glatzmaier (2012) recently used an observational estimate of absolute surface dynamic height obtained from a combination of satellite altimetry and other data to compute Lagrangian regime boundaries in the CCS region under a geostrophic velocity approximation (**Figure 11**). They used a variety of bootstrapping approaches to estimate the sensitivity of the FTLE/FTLS calculation to noise in the observed velocity field and then compared the results of the PLS-line approach to coherent-structure identification with those obtained using an alternative approach based on the Okubo-Weiss criterion (Okubo 1970, Weiss 1991).

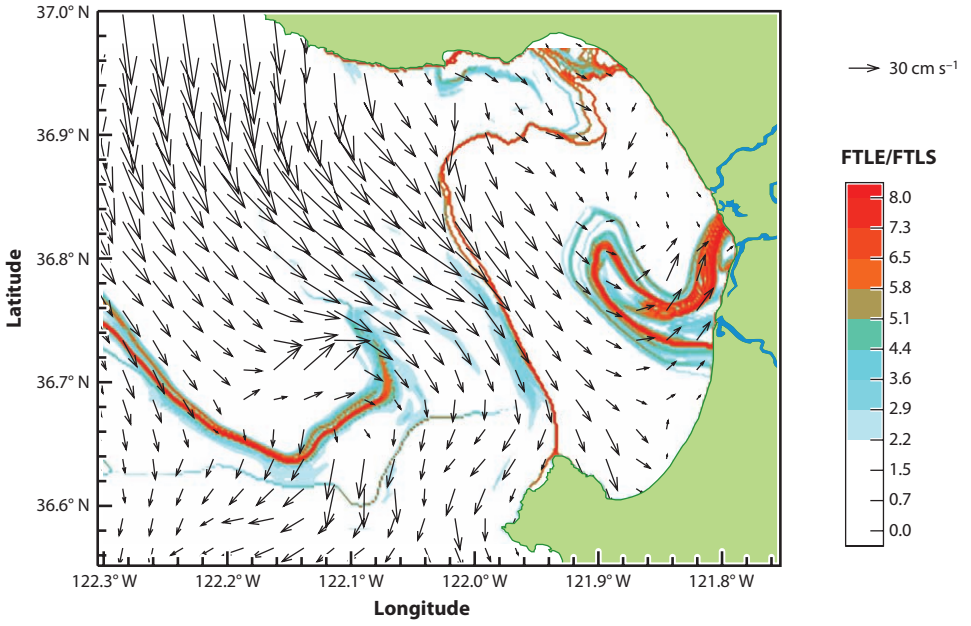

Figure 9

Fixed-time Lyapunov exponent/Lagrangian strain (FTLE/FTLS) field computed from high-frequency radar velocity data in Monterey Bay, California. Curves of high FTLE/FTLS represent time-varying principal Lagrangian strain (PLS) lines. A high-frequency radar velocity field at the given time is also shown. Adapted from Shadden et al. (2009) with permission from Elsevier.

The Okubo-Weiss criterion depends on the parameter s_{OW}^2 in Equation 8, which is computed not from a Lagrangian quantity but rather from the instantaneous velocity gradient tensor. As such, it differs fundamentally from the FTLE/FTLS approach, and from all other parcel and bundle schemes as defined here. The idea of the Okubo-Weiss criterion—as used, for example, by Harrison & Glatzmaier (2012)—is simply that large contiguous regions where $s_{OW}^2 < 0$ may be identified as coherent vortical structures. Harrison & Glatzmaier (2012) found a qualitative correspondence between coherent-structure boundaries indicated by the zero contours of s_{OW}^2 and Lagrangian regime boundaries indicated by the FTLE/FTLS approach. They found empirically that the FTLE/FTLS PLS lines are more robust to noise in the velocity field than the s_{OW}^2 zero contours, an advantage that they attributed to the smoothing inherent in the Lagrangian-mean FTLE/FTLS calculations. They argued that for the expected amplitude of errors in the observationally based velocity field, the FTLE/FTLS method should give reliable estimates of the boundary locations of the larger eddies and stronger jets typically observed in the CCS region, but not those of the smaller eddies or weaker jets.

5.4. A Global Snapshot

For the global ocean, Beron-Vera et al. (2008) have presented results that are similar to those presented by Harrison & Glatzmaier (2012) for the CCS region. Beron-Vera et al.'s (2008) results are, as the authors note, essentially a demonstration of feasibility and as such are less systematic than those of Harrison & Glatzmaier (2012). Beron-Vera et al. (2008) showed that a snapshot of the FTLE/FTLS field over the global ocean can be computed from an altimeter-based data

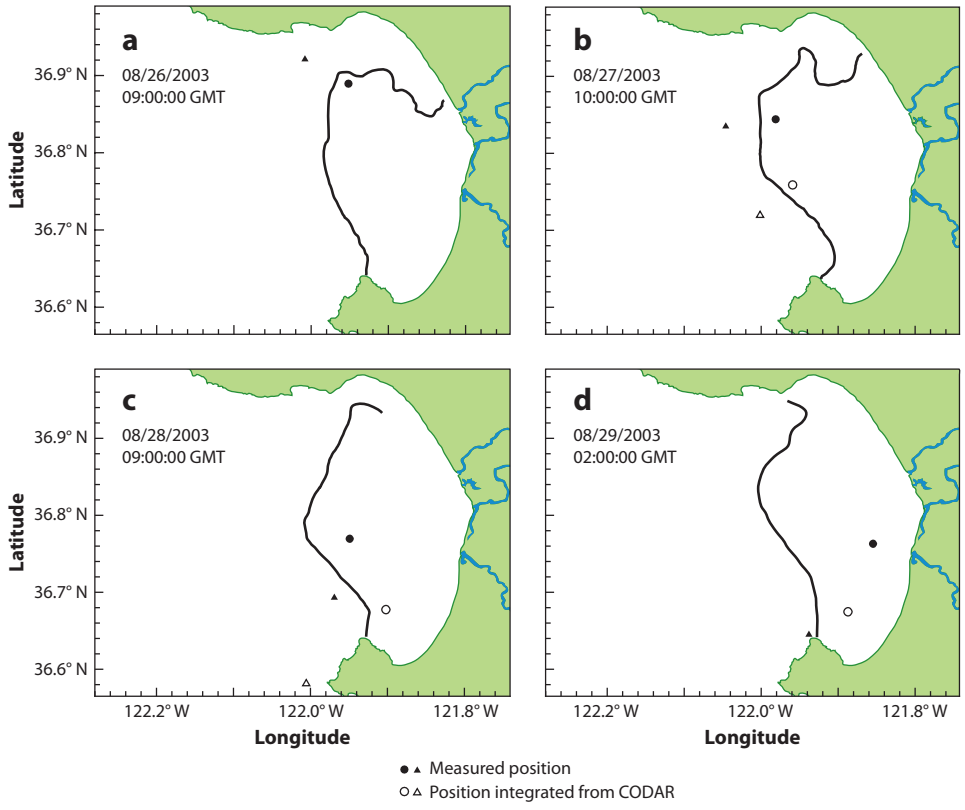

Figure 10

Sequence of observed locations over several days of two drifters (*circles* and *triangles*) in Monterey Bay, California, superimposed with a time-dependent principal Lagrangian strain (PLS) line. Abbreviation: CODAR, coastal ocean dynamics applications radar. Adapted from Shadden et al. (2009) with permission from Elsevier. Time information for the sequence, missing from Shadden et al. (2009), has been added.

set (**Figure 12**). For this snapshot, they used a Lagrangian integration time of $\tau = 60$ days. They then compared their FTLE/FTLS structures in this snapshot with contours of s_{OW}^2 in a single limited region, and argued based on the comparison that the FTLE/FTLS metric is more sensitive and informative. They also argued that the FTLE/FTLS structures indicate that coherent vortical eddy structures identified from closed sea-surface height contours or by the Okubo-Weiss criterion generally do not trap and transport fluid, but this assertion was apparently made on the relatively limited basis of a comparison of a few FTLE/FTLS structures with instantaneous sea-surface height or s_{OW}^2 parameters. They further compared a set of time-dependent FTLE/FTLS structures with a single satellite-tracked drifter and suggested that the results were consistent with the assumption that the FTLE/FTLS structures represented attracting (normally convergent) material curves.

5.5. Numerical Models

The development of high-resolution numerical models of regional and coastal ocean circulation over the past decade (e.g., Samelson et al. 2008, Hasumi et al. 2010, Hurlburt et al. 2011), with

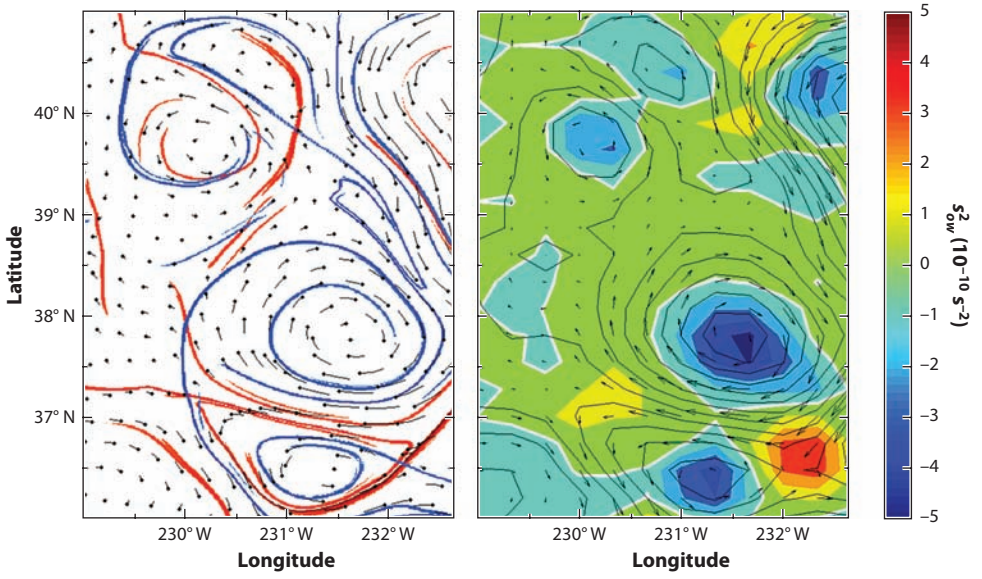

Figure 11

Coherent structures and regime boundaries in the California Current region on October 18, 2005, from an observationally based velocity field. (*a*) Normally convergent (*blue*) and divergent (*red*) principal Lagrangian strain (PLS) lines, with two-day, time-centered trajectories (*black lines*); the circles indicate the final positions. (*b*) Contours of sea-surface height, geostrophic velocity vectors, and the Okubo-Weiss parameter (s^2_{OW}). The sea-surface height contour interval is 3 cm, and the maximum fluid velocity is 35 cm s^{-1}. Dark blue regions indicate elliptical trajectories (high vorticity), and yellow and orange regions indicate areas of high shear near instantaneous stagnation points. White lines indicate s^2_{OW} zero contours. Adapted from Harrison & Glatzmaier (2012) with permission from Taylor & Francis Ltd.

horizontal grid resolutions of order 1–5 km or less, has opened up new opportunities for the diagnosis of PLS lines in increasingly realistic model representations of regional and coastal ocean flows. To the extent that these models are constrained by data assimilation or by a largely deterministic dynamical response to known forcing, the resulting Lagrangian regime boundaries and PLS lines may be descriptive not only in a qualitative and general sense but also in a quantitative and particular sense, as approximate representations or predictions of specific, observable ocean features. Recent modeling analyses of this type include those of d'Ovidio et al. (2004), Mezič et al. (2010), and Rypina et al. (2010).

In the earliest of these latter studies, d'Ovidio et al. (2004) used velocity fields obtained from a numerical model of the Mediterranean Sea (Dietrich 1997, Fernández et al. 2005) to compute PLS lines by the FSLE/FSLS method. The model had a 10-km horizontal grid resolution, adequate to reproduce many of the larger characteristic mesoscale features of Mediterranean circulation, such as the so-called Algerian eddies. A time average of the FSLE/FSLS field suggested higher mesoscale stirring activity in the southern part of the basin. The main object of this work was to introduce the FSLE/FSLS concept and approach into the oceanographic context; the authors reported only limited qualitative and quantitative results, and made no comparisons with observations. The study served to demonstrate the feasibility of an FSLE/FSLS-based approach for identifying PLS lines in a regional ocean model.

The more recent studies by Mezič et al. (2010) and Rypina et al. (2010) were based on models of circulation for the Gulf of Mexico and the Philippine Archipelago, respectively. The latter used an

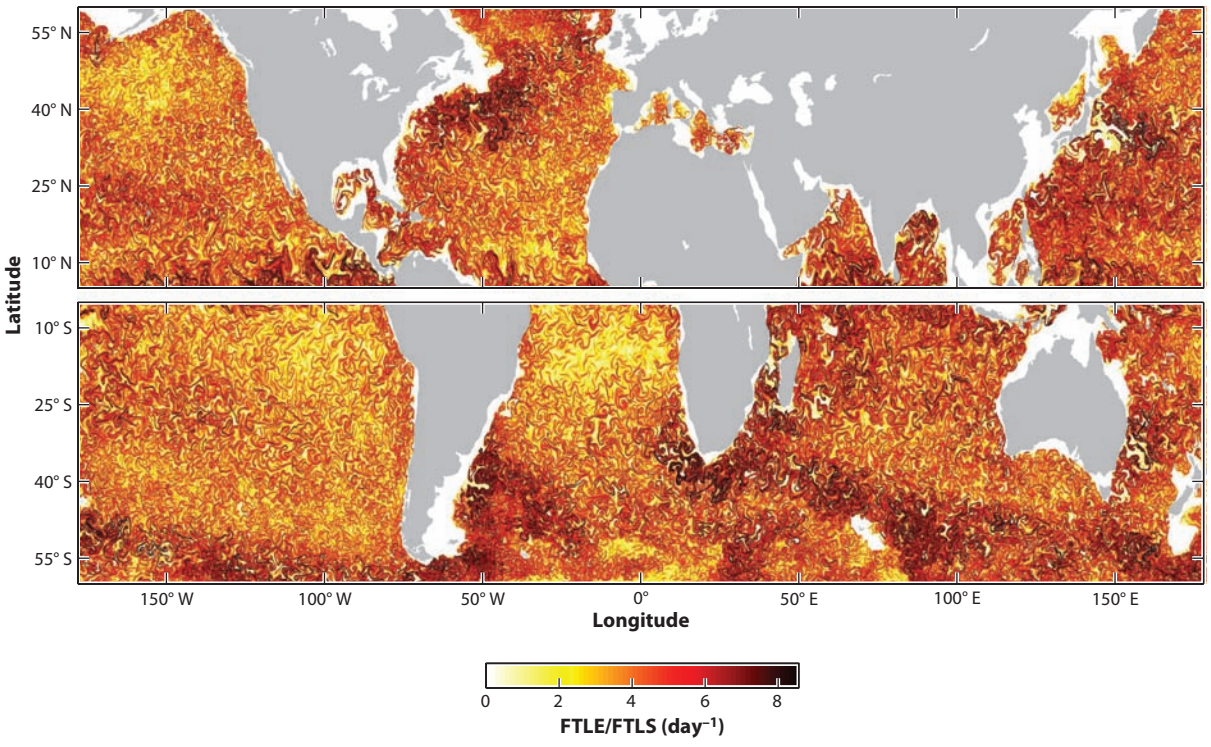

Figure 12

Global snapshot of a backward-time finite-time Lyapunov exponent/Lagrangian strain (FTLE/FTLS) field on April 20, 2005, computed using sea-surface velocities inferred from climatological hydrography and altimetry. Principal Lagrangian strain (PLS) lines correspond to regions with the darkest red tones. Adapted from Beron-Vera et al. (2008) with permission.

FTLE/FTLS scheme, whereas the former introduced a mesohyperbolicity (meaning "hyperbolic on average") bundle scheme based on the spatial gradient (tensor) with respect to the initial position of the average Lagrangian velocity appearing in the parcel scheme of Malhotra et al. (1998). The latter gradient is essentially equivalent to the deformation gradient (tensor) that is used to compute the Cauchy-Green tensor for the FTLE/FTLS scheme, so the mesohyperbolicity quantity is very closely related to FTLE/FTLS; Mezič et al. (2010) explicitly showed the analytical relation between the two quantities in their supporting online material.

For their mesohyperbolicity analysis, Mezič et al. (2010) used velocity fields obtained from a publicly available, quasi-operational, regional numerical model of the Gulf of Mexico circulation (HYCOM GOM10.04, supported by the US Naval Research Laboratory and Naval Oceanographic Office); this model assimilates satellite sea-surface height and temperature and is forced by surface winds and air-sea fluxes from an operational weather forecast model, the US Navy Operational Global Atmospheric Prediction System (NOGAPS). They argued that the resulting PLS-line structures obtained as extrema of the contoured mesohyperbolicity fields give useful predictive information for the observed coastal incursions of oil from the massive Deepwater Horizon blowout spill off Louisiana in the summer of 2010 (**Figure 13**). Huntley et al. (2011) and Olascoaga & Haller (2012) explored related ideas in the same context.

For their FTLE/FTLS analysis, Rypina et al. (2010) used velocity fields obtained from two dedicated regional numerical models of the Philippine Archipelago circulation with approximately

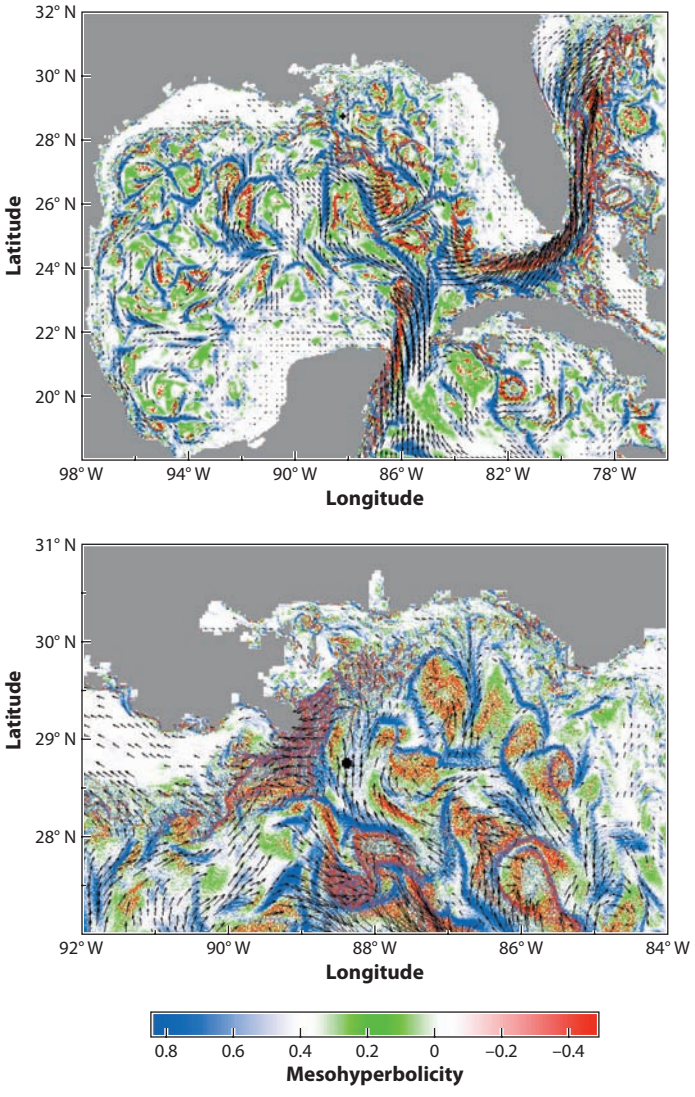

Figure 13

(*a*) Hyper-graph map showing mesohyperbolic (*red* and *blue*) and mesoelliptic (*green*) Lagrangian-mean strain regions on June 25, 2010, computed from model surface velocities over three days, for (*a*) the Gulf of Mexico and (*b*) a coastal subdomain offshore of Plaquemines Parish, Louisiana. Adapted from Mezič et al. (2010) with permission from AAAS.

3-km and 6-km horizontal resolutions, respectively. They did not carry out any data assimilation for the regional models, but the open boundary condition information was taken from a data-assimilating global operational model, and the regional models were forced by air-sea fluxes computed using NOGAPS atmospheric fields. They argued that the PLS lines identified by the FTLE/FTLS analysis (**Figures 14** and **15**) provide a useful framework in which to interpret the mechanisms of mesoscale horizontal stirring and exchange within the archipelago domain. They made a brief comparison with an observed in situ near-surface temperature transect and noted

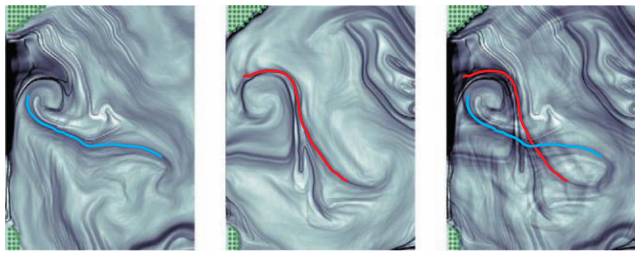

Figure 14

(*a*) Stable manifolds (*blue curves*) and (*b*) unstable manifolds (*red curves*) grown using a direct manifold evolution method by releasing particles in the vicinity of a stagnation-point analog located between two eddies in the western Sulu Sea. The background shading in panels *a* and *b* respectively indicates the forward- and backward-time finite-time Lyapunov exponent/Lagrangian strain (FTLE/FTLS) values [principal Lagrangian strain (PLS) rates]. (*c*) Superimposed results of panels *a* and *b*. In all three panels, green dots indicate land areas. Adapted from Rypina et al. (2010) with permission; original figure copyright © 2010 by the American Meteorological Society.

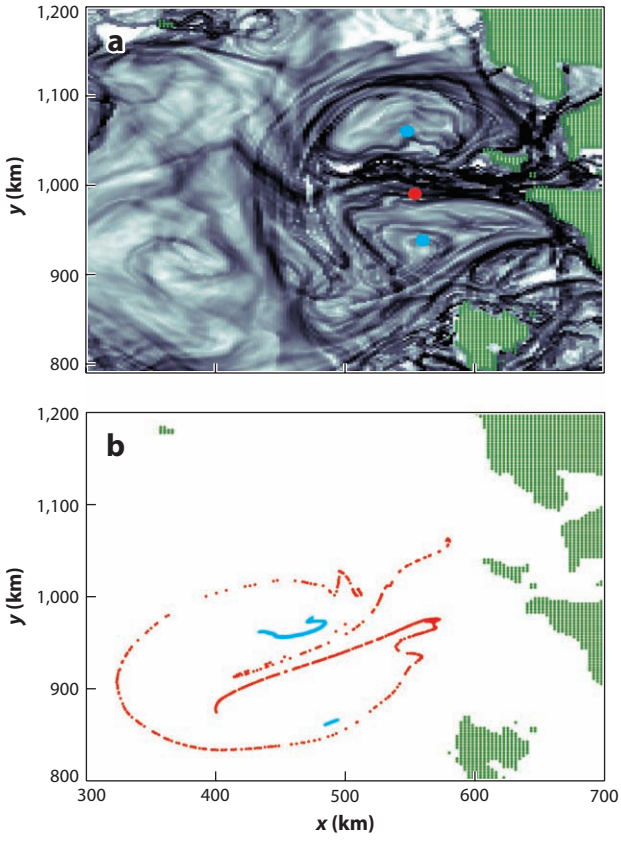

Figure 15

Evolution of patches of surface drifters launched in eddy cores (*blue*) and in a region densely covered by intersecting principal Lagrangian strain (PLS) lines (*red*) over a period of 10 days. (*a*) The PLS lines and drifter patches on January 3, 2005. (*b*) The drifter patches 10 days later. In both panels, green dots indicate land areas. Adapted from Rypina et al. (2010) with permission; original figure copyright © 2010 by the American Meteorological Society.

some suggestive filamentary fluctuations along the edge of a recirculatory eddy, but found the data insufficient to confirm or disprove the predicted presence of the PLS line.

6. VORTICITY-DYNAMICAL COHERENT STRUCTURES

The existence of coherent, organized structures in otherwise quasi-random, turbulent flows has long been recognized (Hussain 1983, McWilliams 1984). Although a rigid definition does not exist, these structures have generally been described as contiguous fluid regions with phase-correlated vorticity and a size comparable to the transverse extent of the shear layer or another characteristic mean-flow scale.

There are many examples of the identification of vortical coherent structures—commonly termed eddies—in the ocean. The most comprehensive recent global compendia, which include numerous citations of related regional studies, are those of Chelton et al. (2007, 2011). In these two studies, the authors used eddy-tracking methods based on the Okubo-Weiss parameter and based directly on the sea-surface height field, respectively, to identify large sets of long-lived eddies in a nearly two-decade, global, satellite-altimeter sea-surface height data set. Chelton et al. (2011) found more than 17,000 such eddies with lifetimes of six months or longer (**Figure 16**). Furthermore, they estimated that the majority of these eddies have fluid velocities U that exceed the corresponding eddy translation speed c, so that $U/c > 1$, which implies that the translating eddy will trap and transport fluid as it moves. Idealized quasi-geostrophic modeling of eddies initialized with scales and amplitudes characteristic of the observed eddies supports the hypotheses that these vortical features can remain coherent for as long as two years or more and trap and transport fluid in their cores (**Figure 17**) (Early et al. 2011). Numerous examples exist of freely drifting surface

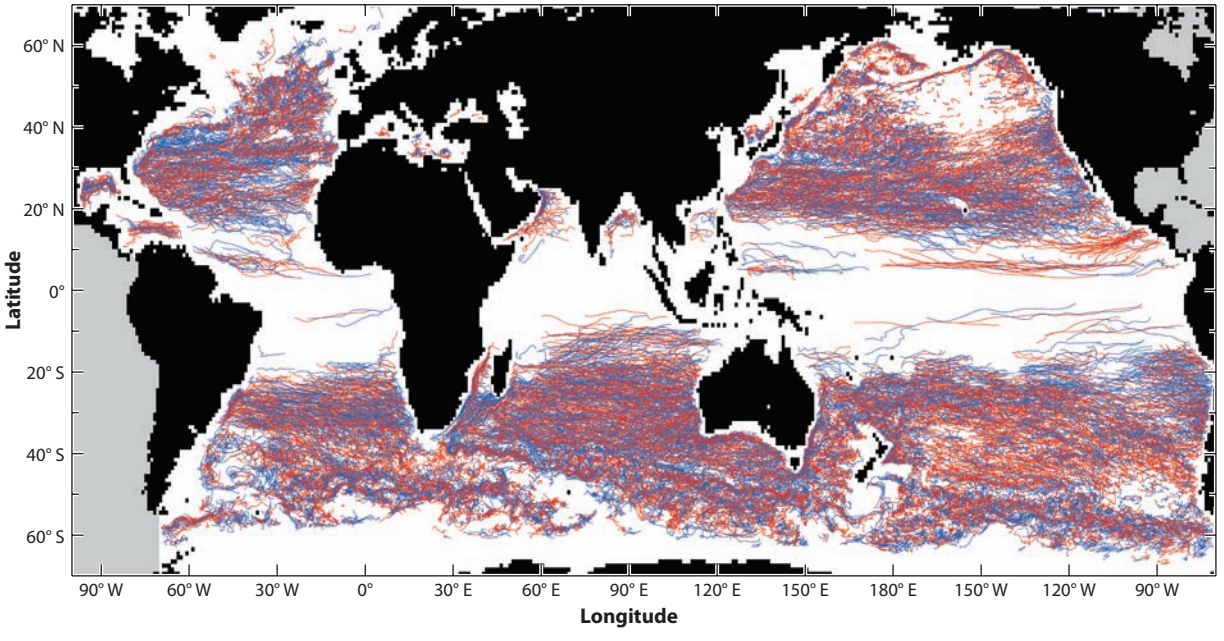

Figure 16

Trajectories of 8,779 cyclonic eddies (*blue lines*) and 8,473 anticyclonic eddies (*red lines*) with lifetimes of at least 26 weeks as identified from satellite sea-surface height fields over a 16-year period from October 1992 to December 2008. Adapted from Chelton et al. (2011) with permission from Elsevier.

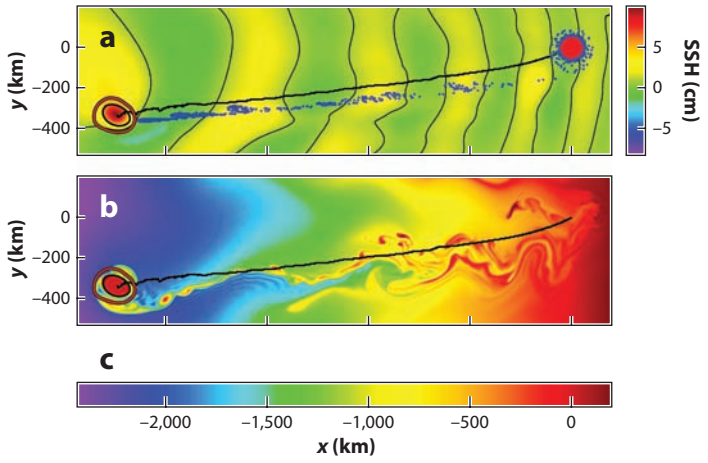

Figure 17

Sea-surface height (SSH) and passive tracer fields from a 675-day quasi-geostrophic numerical simulation of a westward-propagating localized eddy coherent structure versus zonal (*x*) and meridional (*y*) distance. (*a*) SSH along with the instantaneous trapped fluid contour (*red*) and relative vorticity zero contour (*black*). The initial and final locations of fluid parcels around the eddy perimeter (*blue circles*) and in the eddy core (*red circles*) are also shown. (*b*) Final (day-675) distribution of a scalar passive tracer equal to the initial (day-0) value of the zonal coordinate. (*c*) Initial distribution of the scalar passive tracer (initial zonal coordinate) for which the final distribution is shown in panel *b*. The zonal axes are the same across all three panels. Adapted from Early et al. (2011) with permission; original figure copyright © 2011 by the American Meteorological Society.

or subsurface ocean instruments that appear to be trapped in and transported by such features (e.g., **Figure 18**) (Margolina et al. 2006). These analyses argue for the widespread presence of vortical coherent structures and trapped Lagrangian fluid motion throughout much of the global ocean.

This oceanographically important and now classical idea of a vortical coherent structure in a turbulent flow differs from the concept of a PLS line in several essential ways. As noted in Section 4.1, it is because of the associated possibility for confusion that the PLS terminology is used here rather than the LCS alternative. The classical, dynamical coherent structures are associated with specific vorticity features, where vorticity is an essential dynamical element of both three-dimensional turbulence and large-scale geophysical fluid flow. At least in principle, the classical vortical coherent structure can be identified in an instantaneous velocity (vorticity) field. In contrast, the PLS line is not directly related to the instantaneous dynamical fluid fields, and can be identified only by computing Lagrangian motion over long time intervals. In addition, the rotating, stratified dynamics of geophysical fluid flow often include both an approximate material conservation law for a vorticity (or potential vorticity) quantity and an approximate balance relation connecting the velocity field to the conserved vorticity quantity. This leads in a direct and very general physical way to the quasi-stability of isolated, coherent vortex structures (e.g., Flierl 1987), a property that is sufficiently robust to allow representation of some basic dynamical processes in terms of the interaction of point vortices (e.g., Zabusky & McWilliams 1985). In contrast, the occurrence of persistent strain along a material trajectory or curve appears to be, from a dynamical point of view, almost accidental; in general, there is no approximate material conservation law for strain in geophysical or classical turbulent fluid flow. Thus, there is little evidence that strain fields typically possess or induce the intrinsic dynamical stability or structural coherence that might

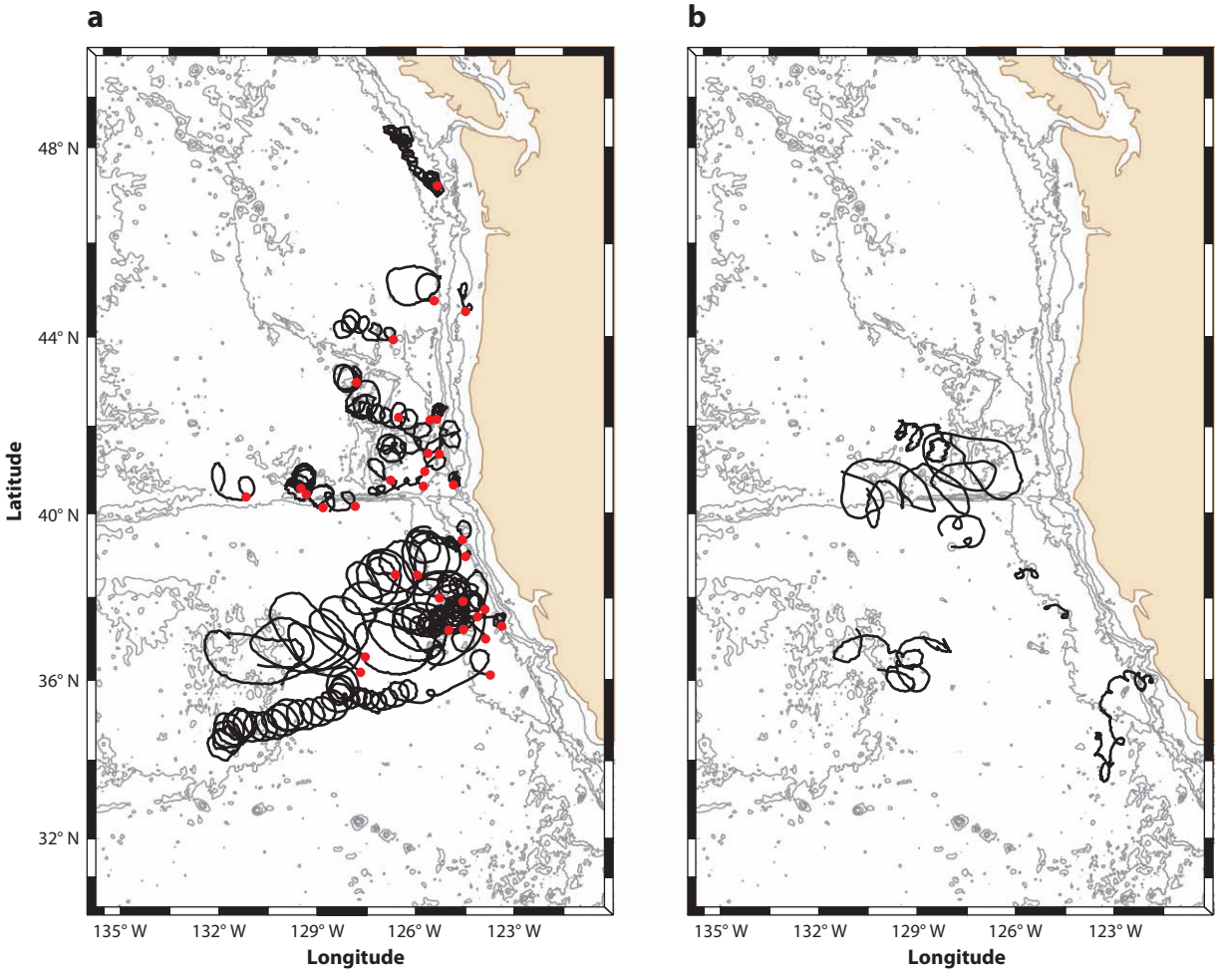

Figure 18

(*a*) Anticyclonic and (*b*) cyclonic looping trajectories from freely drifting subsurface RAFOS floats deployed in the California Current System. Red dots show where a float appears to have been entrained by a coherent eddy structure. Adapted from Margolina et al. (2006) with permission.

seem to be implied by the characterization of lines of persistent material strain—PLS lines and points—as coherent (Lagrangian) structures.

7. SUMMARY

It has been two decades since the recognition that the separatrix trajectories familiar from analytical mechanics and the geometric theory of ordinary differential equations are useful objects of study in simplified models of Lagrangian motion in specific ocean flow regimes. There are many important aspects of the analysis of Lagrangian motion in the ocean that have developed independently and have not been influenced by this perspective (e.g., see the variety of approaches represented in Griffa et al. 2007), but there is certainly no doubt that, at a minimum, the subsequent work in this area has produced advances in our ability to define and identify generalized analogs of these

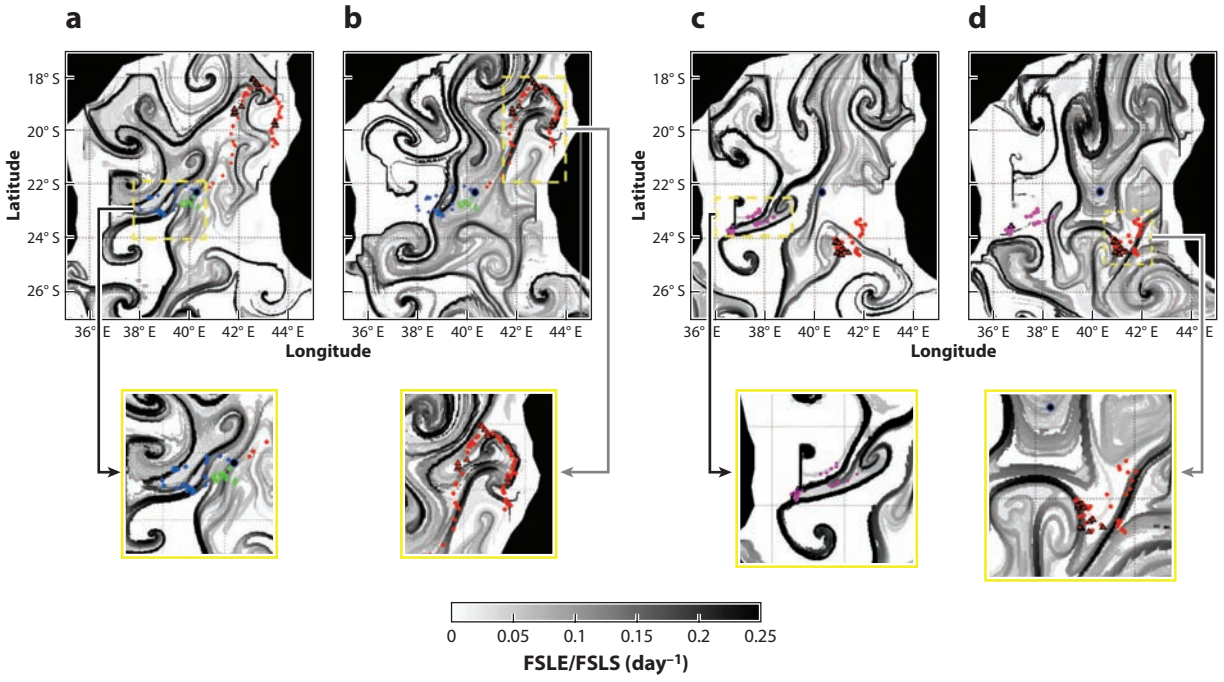

Figure 19

Overlays of seabird positions on principal Lagrangian strain [finite-size Lyapunov exponent/Lagrangian strain (FSLE/FSLS)] maps. (*a*,*c*) Backward-time FSLE/FSLS values (day^{-1}). (*b*,*d*) Forward-time FSLE/FSLS values (day^{-1}). Panels *a* and *b* are for the week of September 24, 2003; panels *c* and *d* are for the week of October 6, 2003. Circles represent seabird trajectories, and triangles represent foraging patches; each color represents the tag of a different bird. Adapted from Tew Kai et al. (2009) with permission; original figure copyright © 2009 by the National Academy of Sciences.

Lagrangian regime-boundary trajectories in observational estimates of ocean flow fields and in various increasingly complex and sophisticated numerical models of ocean circulation.

A personal point of reference is an early review of these ideas by this author (Samelson 1996). Several of the open issues discussed in that review have since been resolved, generally in favor of the new perspective. Perhaps most notably, Rogerson et al. (1999) and others have shown that the qualitative picture of Lagrangian motion suggested by kinematic models such as the traveling-wave flow (Equation 1) is fundamentally correct for dynamical fluid motions with an approximate vorticity or potential vorticity conservation law. These studies have also established the dynamical tendency to homogenize potential vorticity along regime boundaries, as anticipated by Samelson (1996) and others. Studies of idealized critical layers have been carried out in this context (e.g., Ngan & Shepherd 1997) and have confirmed some of the speculations of Samelson (1996), but more attention has been given to the analysis of general ocean flows with eddy or other dynamical coherent structures, as indicated by the brief survey given here (Section 4). In some cases, connections have even been made to biological signatures or processes associated with features identified by these analyses (e.g., **Figure 19**) (Tew Kai et al. 2009).

A recent subtle shift in this work has been a somewhat reduced attention to the identification of flow-regime boundaries for dynamical coherent structures and a somewhat increased attention to the identification of lines of large Lagrangian-mean strain (PLS lines, or LCSs) as objects of immediate interest. This shift seems to be partly the result of the recognition that the lines or

regions of large Lagrangian-mean strain have particular interest as sites of intensive horizontal stirring and mixing of fluid properties, and partly the result of the practical availability of methods to compute PLS quantities that are relatively standard and straightforward (e.g., Ottino 1989, Pierrehumbert & Yang 1993, Haller 2001, Shadden et al. 2005), in contrast, for example, to the more phenomenologically specific methods that must typically be used to identify dynamical coherent structures (e.g., Chelton et al. 2007, 2011).

In either case, the most success for the analysis of these features in complicated velocity fields has been obtained through the basic step of moving from the direct identification of isolated analogs of stagnation points to a contoured-field approach that uses local extrema of Lagrangian-mean quantities to identify the candidate regime boundaries or PLS lines. In this sense, tangible progress has clearly been made, and it seems likely that computational methods of this general type will dominate the future of oceanographic Lagrangian regime-boundary and Lagrangian-mean strain analysis. However, many of the achievements in the oceanographic literature relate only to establishing the existence of these Lagrangian features in progressively more complex modeled or observed flows. The basic conceptual insights offered by the simple original models have been largely confirmed, and to some extent given a more quantitative foundation, for the more general flows considered in the subsequent work. Beyond this confirmation, however, it is not easy to find major advances in the physical understanding of oceanic motions that have originated with this approach. Perhaps this is an indication that the tools are still new and the best results are yet to come.

DISCLOSURE STATEMENT

The author is not aware of any affiliations, memberships, funding, or financial holdings that might be perceived as affecting the objectivity of this review.

ACKNOWLEDGMENTS

Preparation of this review was supported by the Office of Naval Research (grant N00014-09-1-0268) and the National Aeronautics and Space Administration (grant NNX08AR37G).

LITERATURE CITED

Aurell E, Boffetta G, Crisanti A, Paladin G, Vulpiani A. 1997. Predictability in the large: an extension of the concept of Lyapunov exponent. *J. Phys. A* 30:1–26

Beron-Vera FJ, Olascoaga MJ, Goni GJ. 2008. Oceanic mesoscale eddies as revealed by Lagrangian coherent structures. *Geophys. Res. Lett.* 35:L12603

Bishop RL, Goldberg SI. 1980. *Tensor Analysis on Manifolds*. New York: Dover

Bower AS. 1991. A simple kinematic mechanism for mixing fluid parcels across a meandering jet. *J. Phys. Oceanogr.* 21:173–80

Bower AS, Rossby HT. 1989. Evidence of cross-frontal exchange processes in the Gulf Stream based on isopycnal RAFOS float data. *J. Phys. Oceanogr.* 19:1177–90

Chelton DB, Schlax MG, Samelson RM. 2011. Global observations of nonlinear mesoscale eddies. *Prog. Oceanogr.* 91:167–216

Chelton DB, Schlax MG, Samelson RM, de Szoeke RA. 2007. Global observations of large oceanic eddies. *Geophys. Res. Lett.* 34:L15606

Coulliette C, Lekien F, Paduan J, Haller G, Marsden J. 2007. Optimal pollution mitigation in Monterey Bay based on coastal radar data and nonlinear dynamics. *Environ. Sci. Technol.* 41:6562–72

Dietrich DE. 1997. Application of a modified Arakawa "A" grid ocean model having reduced numerical dispersion to the Gulf of Mexico circulation. *Dyn. Atmos. Oceans* 27:201–17

d'Ovidio F, Fernández V, Hernández-Garcia E, López C. 2004. Mixing structures in the Mediterranean sea from finite size Lyapunov exponents. *Geophys. Res. Lett.* 31:L17203

Early JJ, Samelson RM, Chelton DB. 2011. The evolution and propagation of quasi-geostrophic ocean eddies. *J. Phys. Oceanogr.* 41:1535–55

Fernández V, Dietrich DE, Haney RL, Tintoré J. 2005. Mesoscale, seasonal and interannual variability in the Mediterranean Sea using a numerical ocean model. *Prog. Oceanogr.* 66:321–40

Flierl G. 1981. Particle motions in large-amplitude wave fields. *Geophys. Astrophys. Fluid Dyn.* 18:39–74

Flierl G. 1987. Isolated eddy models in geophysics. *Annu. Rev. Fluid Mech.* 19:493–530

Griffa A, Kirwan AD Jr, Mariano A, Özgökmen T, Rossby T, eds. 2007. *Lagrangian Analysis and Prediction of Coastal and Ocean Dynamics.* New York: Cambridge Univ. Press

Guckenheimer J, Holmes P. 1983. *Nonlinear Oscillations, Dynamical Systems, and Bifurcations of Vector Fields.* New York: Springer-Verlag

Haller G. 2000. Finding finite-time invariant manifolds in two-dimensional velocity fields. *Chaos* 10:99–108

Haller G. 2001. Distinguished material surfaces and coherent structure in three-dimensional fluid flows. *Physica D* 149:248–77

Haller G. 2002. Lagrangian coherent structures from approximate velocity data. *Phys. Fluids* 14:1851–61

Haller G. 2011. A variational theory of hyperbolic Lagrangian Coherent Structures. *Physica D* 240:574–98

Haller G, Sapsis T. 2011. Lagrangian coherent structures and the smallest finite-time Lyapunov exponent. *Chaos* 21:023115

Haller G, Yuan G. 2000. Lagrangian coherent structures and mixing in two-dimensional turbulence. *Physica D* 147:352–70

Harrison C, Glatzmaier G. 2012. Lagrangian coherent structures in the California Current System—sensitivities and limitations. *Geophys. Astrophys. Fluid Dyn.* 106:22–44

Hasumi H, Tatebe H, Kawasaki T, Kurogi M, Sakamoto TT. 2010. Progress of North Pacific modeling over the past decade. *Deep-Sea Res. II* 57:1188–200

Huntley HS, Lipphardt BL Jr, Kirwan AD Jr. 2011. Surface drift predictions of the Deepwater Horizon spill: the Lagrangian perspective. In *Monitoring and Modeling the Deepwater Horizon Oil Spill: A Record-Breaking Enterprise*, Geophys. Monogr. Ser. 195, ed. Y Liu, A MacFadyen, Z-G Ji, RH Weisberg, pp. 179–95. Washington, DC: Am. Geophys. Union

Hurlburt HE, Metzger EJ, Richman JG, Chassignet EP, Drillet Y, et al. 2011. Dynamical evaluation of ocean models using the Gulf Stream as an example. In *Observing, Assimilating, and Forecasting the Ocean*, ed. A Schiller, G Brassington, pp. 545–609. New York: Springer

Hussain AKMF. 1983. Coherent structures—reality and myth. *Phys. Fluids* 26:2816–50

Ide K, Small D, Wiggins S. 2002. Distinguished hyperbolic trajectories in time dependent fluid flows: analytical and computational approach for velocity fields defined as data sets. *Nonlinear Proc. Geophys.* 9:237–63

Knobloch E, Weiss J. 1987. Chaotic advection by modulated traveling waves. *Phys. Rev. A* 36:1522–24

Kuebel Cervantes BT, Allen JS, Samelson RM. 2003. A modeling study of Eulerian and Lagrangian aspects of shelf circulation off Duck, North Carolina. *J. Phys. Oceanogr.* 33:2070–92

Kuebel Cervantes BT, Allen JS, Samelson RM. 2004. Lagrangian characteristics of continental shelf flows forced by periodic wind stress. *Nonlinear Proc. Geophys.* 11:3–16

Leung S. 2011. An Eulerian approach for computing the finite time Lyapunov exponent. *J. Comput. Phys.* 230:3500–24

Lozier MS, Pratt LJ, Rogerson AM, Miller PD. 1997. Exchange geometry revealed by float trajectories in the Gulf Stream. *J. Phys. Oceanogr.* 27:2327–41

Madrid J, Mancho AM. 2009. Distinguished trajectories in time dependent vector fields. *Chaos* 19:013111

Malhotra N, Mezič I, Wiggins S. 1998. Patchiness: a new diagnostic for Lagrangian trajectory analysis in time-dependent fluid flows. *Int. J. Bifurc. Chaos* 8:1053–93

Mancho A, Small D, Wiggins S. 2004. Computation of hyperbolic and their stable and unstable manifolds for oceanographic flows represented as data sets. *Nonlinear Proc. Geophys.* 11:17–33

Mancho A, Small D, Wiggins S. 2006. A tutorial on dynamical systems concepts applied to Lagrangian transport in oceanic flows defined as finite time data sets: theoretical and computational issues. *Phys. Rep.* 437:55–124

Mancho A, Small D, Wiggins S, Ide K. 2003. Computation of stable and unstable manifolds of hyperbolic trajectories in two-dimensional, aperiodically time-dependent vector fields. *Physica D* 182:188–222
Margolina T, Collins CA, Rago TA, Paquette RG, Garfield N. 2006. Intermediate level Lagrangian subsurface measurements in the northeast Pacific: isobaric RAFOS float data. *Geochem. Geophys. Geosyst.* 7:Q09002
Mathur M, Haller G, Peacock T, Ruppert-Felsot JE, Swinney HL. 2007. Uncovering the Lagrangian skeleton of turbulence. *Phys. Rev. Lett.* 98:144502
McWilliams JC. 1984. The emergence of isolated coherent vortices in turbulent flow. *J. Fluid Mech.* 146:21–43
Mendoza C, Mancho AM. 2010. Hidden geometry of ocean flows. *Phys. Rev. Lett.* 105:038501
Mezič I, Loire S, Fonoberov V, Hogan P. 2010. A new mixing diagnostic and gulf oil spill movement. *Science* 330:486–89
Ngan K, Shepherd TG. 1997. Chaotic mixing and transport in Rossby wave critical layers. *J. Fluid Mech.* 334:315–51
Okubo A. 1970. Horizontal dispersion of floatable particles in the vicinity of velocity singularities such as convergences. *Deep-Sea Res.* 17:445–54
Olascoaga M, Haller G. 2012. Forecasting sudden changes in environmental pollution patterns. *Proc. Natl. Acad. Sci. USA* 109:4738–43
Oseledec V. 1968. A multiplicative ergodic theorem: Lyapunov characteristic numbers for dynamical systems. *Trans. Mosc. Math. Soc.* 19:197–231
Ottino J. 1989. *The Kinematics of Mixing: Stretching, Chaos, and Transport*. Cambridge: Cambridge Univ. Press
Paduan J, Rosenfeld L. 1996. Remotely sensed surface currents in Monterey Bay from shore-based HF radar (Coastal Ocean Dynamics Application Radar). *J. Geophys. Res.* 101:20669–86
Pierrehumbert RT. 1991. Chaotic mixing of tracer and vorticity by modulated traveling Rossby waves. *Geophys. Astrophys. Fluid Dyn.* 58:285–319
Pierrehumbert RT, Yang H. 1993. Global chaotic mixing on isentropic surfaces. *J. Atmos. Sci.* 50:2462–80
Rogerson AM, Miller PD, Pratt LJ, Jones CKRT. 1999. Lagrangian motion and fluid exchange in a barotropic meandering jet. *J. Phys. Oceanogr.* 29:2635–55
Rypina I, Pratt L, Pullen J, Levin J, Gordon A. 2010. Chaotic advection in an archipelago. *J. Phys. Oceanogr.* 40:1988–2006
Samelson RM. 1992. Fluid exchange across a meandering jet. *J. Phys. Oceanogr.* 22:431–40
Samelson RM. 1996. Chaotic transport by mesoscale motions. In *Stochastic Modelling in Physical Oceanography*, ed. RJ Adler, P Müller, BL Rozovskii, pp. 423–38. Boston: Birkhäuser
Samelson RM, Allen JS, MacCready P. 2008. Progress in coastal ocean modeling during CoOP. *Oceanography* 21(4):136–47
Samelson RM, Wiggins S. 2006. *Lagrangian Transport in Geophysical Jets and Waves*. New York: Springer
Shadden S, Lekien F, Marsden J. 2005. Definition and properties of Lagrangian coherent structures from finite-time Lyapunov exponents in two-dimensional aperiodic flows. *Physica D* 212:271–304
Shadden S, Lekien F, Paduan J, Chavez F, Marsden J. 2009. The correlation between surface drifters and coherent structures based on high-frequency radar data in Monterey Bay. *Deep-Sea Res. II* 56:161–72
Stommel H. 1965. *The Gulf Stream*. Berkeley: Univ. Calif. Press. 248 pp.
Tew Kai E, Rossi V, Sudre J, Weimerskirch H, Lopez C, et al. 2009. Top marine predators track Lagrangian coherent structures. *Proc. Natl. Acad. Sci. USA* 106:8245–50
Weiss J. 1991. The dynamics of enstrophy transfer in two-dimensional hydrodynamics. *Physica D* 48:273–94
Wiggins S. 2005. The dynamical systems approach to Lagrangian transport in oceanic flows. *Annu. Rev. Fluid Mech.* 37:295–328
Zabusky NJ, McWilliams JC. 1982. A modulated point-vortex model for geostrophic, beta-plane dynamics. *Phys. Fluids* 25:2175–82

Annual Review of
Marine Science

Volume 5, 2013

Contents

Errata

An online log of corrections to *Annual Review of Marine Science* articles may be found at http://marine.annualreviews.org/errata.shtml